https://doi.org/10.1016/j.jmps.2017.09.002

Spiral interface: A reinforcing mechanism for laminated composite materials learned from nature

Yang Gao†, Zhenbin Guo†, Zhaoqiang Song, Haimin Yao*
Department of Mechanical Engineering, The Hong Kong Polytechnic University, Hung Hom, Kowloon, Hong Kong

† These authors contribute equally.
* Corresponding author. Fax: +852 2365 4703. E-mail address: mmhyao@polyu.edu.hk (H. Yao)

Abstract:

Helical structures are ubiquitous in nature at length scales of a wide range. In this paper, we studied a helical architecture called microscopic screw dislocation (μ-SD), which is prevalently present in biological laminated composites such as shells of mollusks *P. placenta* and nacre of abalone. Mechanical characterization indicated that μ-SDs can greatly enhance resistance to scratching. To shed light on the underlying reinforcing mechanisms, we systematically investigated the mechanical behaviors of μ-SD using theoretical modelling in combination with finite element simulation. Our analysis on an individual μ-SD showed that the failure of a μ-SD under tension involves the delamination of the prolonged spiral interface, giving rise to much higher toughness compared to those of the planar counterpart. The corporation of multiple μ-SDs was further investigated by analyzing the effect of μ-SD density on the mechanical reinforcement. It was found that higher areal density of μ-SD would lead to more improvement in toughness. However, the operation of such reinforcing mechanism of μ-SD requires proclivity of cracking along the spiral interface, which is not spontaneous but conditional. Fracture mechanics-based modelling indicated that the proclivity of crack propagation along the spiral interface can be ensured if the fracture toughness of the interface is less than 60% of that of the lamina material. These findings not only uncover the reinforcing mechanisms of μ-SDs in biological materials but imply a great promise of applying μ-SDs in reinforcing synthetic laminated composites.

Keywords: Delamination; Microscopic screw dislocation; Biomineralized materials; Bio-inspired materials

1. Introduction

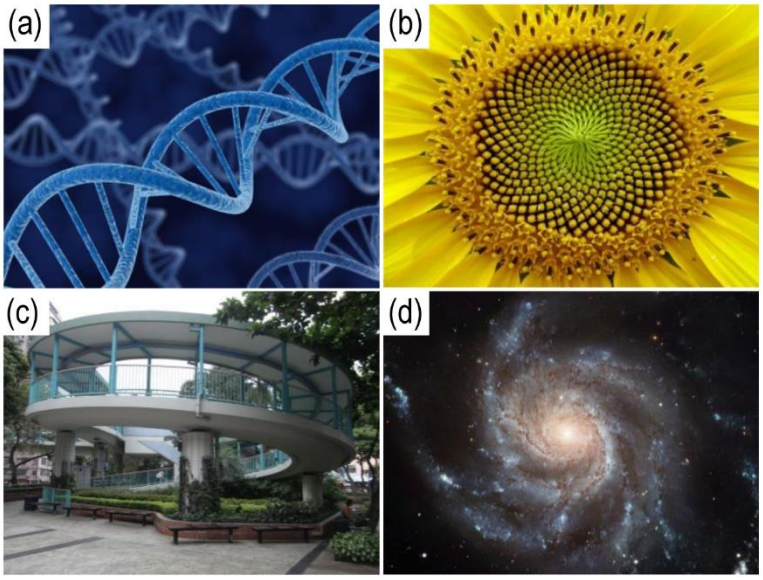

Fig. 1. Spiral structures at multiple length scales. (a) Double-helix of DNA, (b) spiral layout pattern of sunflower seeds, (c) spiral ramp of a garage, and (d) spiral arms of Milky Way galaxy.

Spiral or helix is a ubiquitous structural feature that is observed at length scales of wide range (Fig. 1), from the double helical DNA (Kelley and Barton, 1999; Wang et al., 1979; Watson and Crick, 1953) through the pattern of sunflower seeds (Mathai and Davis, 1974; Vogel, 1979), all the way up to the Milky Way galaxy (Brunthaler et al., 2011; Weinberg, 1992), implying the crucial roles they play in a variety of physical, chemical and biological processes. Recently, a unique microscopic spiral structure in the shells of mollusks of different species has attracted a bunch of attentions from material researchers. For example, the nacre layer of red abalone, which composites the microscopic aragonite tablets and proteins in a well-known "brick-and-mortar" structure (Gao et al., 2003; Ji and Gao, 2004; Shao et al., 2012; Tang et al., 2007), was found to contain some spiral tablets called "screw dislocations" (Yao et al., 2006). These nonplanar tablets interconnect the planar ones on vertically adjacent layers just like a spiral ramp connecting the garages of different floors (Fig. 1(c)). Similar spiral connections were also discovered in the shell of bivalve *Placuna placenta*, which is a laminated composite composed of calcite laminae bonded together by thin layers of organic material (Li and Ortiz, 2015). Unlike the laminae in the traditional laminates (Gibson, 1994) that are parallel and discontinuous in

topology, the calcite laminae in the shell of *P. placenta* are interconnected through a type of spiral structure called "screw dislocation-like connection". While nacre contains ~10^3 "screw dislocations" per square millimeter (Yao et al., 2006), the average areal density of the "screw dislocation-like connections" in the shell of *P. placenta* was reported to be 100-400 mm^{-2} (Li and Ortiz, 2015). The formation mechanism of these biological spiral structures was attributed to the effect of atomistic dislocations on the growth of crystals (Wada, 1966). Preliminary studies on the mechanical functions of these spiral structures indicated that the "screw dislocations" in nacre can enhance the strength by interlocking the vertically adjacent aragonite tablets and therefore constraining their relative motions (Yao et al., 2006). For the shell of *P. placenta*, Li *et al.* demonstrated, from the perspective of energy dissipation and damage localization, that the "dislocation-like connections" can significantly improve the resistance of the shell to the mechanical penetration (Li and Ortiz, 2015). The reinforcement effects of the spiral structures were basically attributed to the role of connection played by the spiral structures. However, if connection is their only function, it may not be necessary for nature to develop such a sophisticated structure; simple micro- pillars or plates are also capable of uniting laminae of different layers in the laminated composite materials. This inference leads us to speculate that the spiral structures in the natural laminated composites may play a role more than a connector. It is noticeable that the use of term "dislocation" in the previous studies seems a misleading metaphor since in materials science dislocation actually refers to a crystallographic defect at atomic length scale (Taylor, 1934). Although the spiral structures introduced above exhibit a quite similar morphology to screw dislocations, they are quite distinct in length scales. While screw dislocations are atomic defects, the spiral connectors are structures at microscopic scale. For distinction, in our discussion below they are designated as "microscopic screw dislocations" or μ-SDs in short.

In this work, we first characterized the mechanical reinforcement effect of the μ-SDs in the shell of *P. placenta* by microscopic scratching tests. Higher resistance to scratching was detected when the probe approaching the centers of μ-SDs. Through finite element-based simulation, we found that such enhancement of resistance to scratching can be attributed to the spiral interface in the μ-SD which

makes the interfacial crack to propagate along a three-dimensional spiral pathway, resulting in much more energy consumption compared to the planar and through counterpart. Subsequent theoretical modeling indicated that such reinforcing mechanism is not a spontaneous feature of the spiral interface. The condition for it to operate was explored and found dependent on the competition between the fracture toughness of the interface and that of the substantial solid phase.

2. Characterization of mechanical reinforcement

Fig. 2(a) shows the shells of *P. placenta* obtained from Shui Dong Bay, South China Sea, which are laminated composites composed of 99 wt% calcite and a small amount of organic material. The thickness of each calcite lamina and organic interlayer are 0.2-0.9 μm (Wang et al., 2001) and 20-30 nm (Meyers et al., 2008; Song et al., 2003; Wang et al., 2001), respectively. Different from the laminae in the traditional laminated composites (Gibson, 1994), the mineral platelets in the shell of *P. placenta* are vertically interconnected through μ-SDs (Li and Ortiz, 2015). These μ-SDs exhibit either right-handed or left-handed helicity. Normally, μ-SDs with opposite helicity appear in pairs, as shown in Fig. 2(b) (Yao et al., 2009).

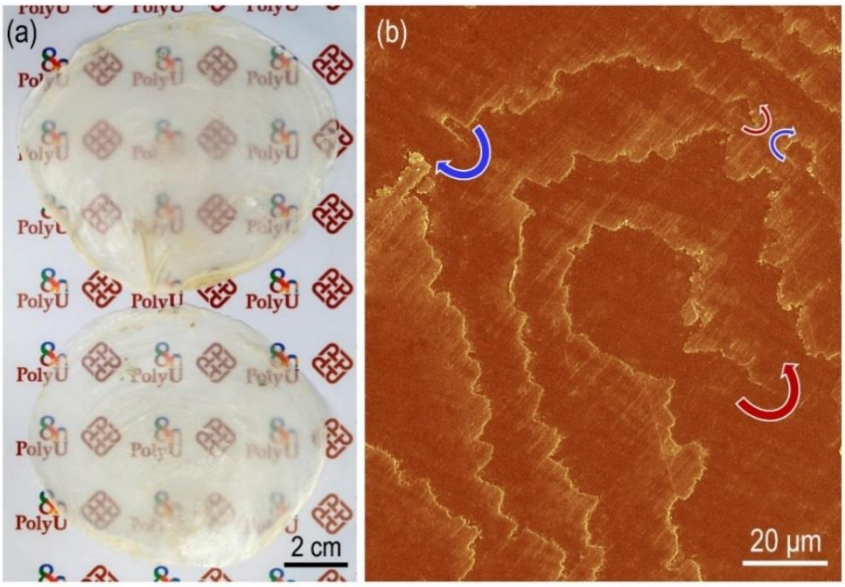

Fig. 2. (a) Translucent shells of *P. placenta.* (b) False-colored SEM image of μ-SDs in the shell of *P. placenta* with opposite helicity.

To evaluate the effect of spiral structure on the mechanical properties of the shell, scratching tests

were carried out on specimens (100 mm × 50 mm × 0.5 mm) incised from the central part of *P. placenta* shells with a precision cutting machine (Minitom, Struers). To minimize the effect of surface roughness on the scratching result, the surfaces of specimens were well polished with a series of sand papers from 400 to 7000 grits and lubrication with deionized (DI) water. Subsequently, samples were rinsed with DI water thoroughly and dried in air. Scratching tests were conducted using a diamond conical probe (Universal Mechanical Tester, Bruker). The scratching path was selected with caution so as to make it pass through center of a μ-SD. To avoid the interference between the adjacent scratches, the inter-scratch spacing was set at least 8 mm, which is more than 100 times of the maximum width of the scratch grooves. To verify the repeatability of the results, 10 mm long scratching was repeated on ten different samples with scratching speed 0.04 mm/s. During the scratching processes, the normal force applied on the probe, F_n, was constantly taken as 0.3 N. The ratio of the measured horizontal resistance force to the fixed normal force, F_r/F_n, was used to depict the resistance of the specimen to scratching.

A typical scratch groove is shown in Fig. 3(a) along with the corresponding wear resistance F_r/F_n. As expected, the scratch groove passes through the center of a μ-SD. The wear resistance, which is characterized by F_r/F_n, reaches the maximum around 0.8 near the μ-SD center and exhibits relatively lower value in the region distant from the μ-SD. Since the sample surface has been well polished and the average groove depth (>15μm，see Fig. 3(b)) is much larger than the thickness of laminae (0.2-0.9 μm (Wang et al., 2001), such elevated wear resistance near the center of the μ-SD should not be attributed to the difference of altitude, if available, between the laminae. A plausible factor accounting for the higher resistance near the μ-SD center is the spiral interfaces between laminae. For a laminated composite under in-plane scratching, cracks (mode-II dominant) form in the front of the probe and propagate as the scratching proceeds. Near a μ-SD, the inter-lamina interface, which normally is weak compared to the lamina material, is no longer planar but spiral. When reaching a μ-SD, cracks have preference in energy to propagate along the spiral interface rather than directly penetrating through the lamina. The prolonged pathway of crack propagation along the spiral interface defers the failure of μ-SD, giving rise to more energy consumption and higher resistance force. Such reinforcing mechanism

of the spiral interface, if works in the scratching tests, is believed also functional in the fracture processes caused by the other mechanical loadings such as uniaxial tension. To verify this hypothesis, finite element analysis (FEA) is carried out to make a comparative study on the behaviors of the laminated composites with and without μ-SDs.

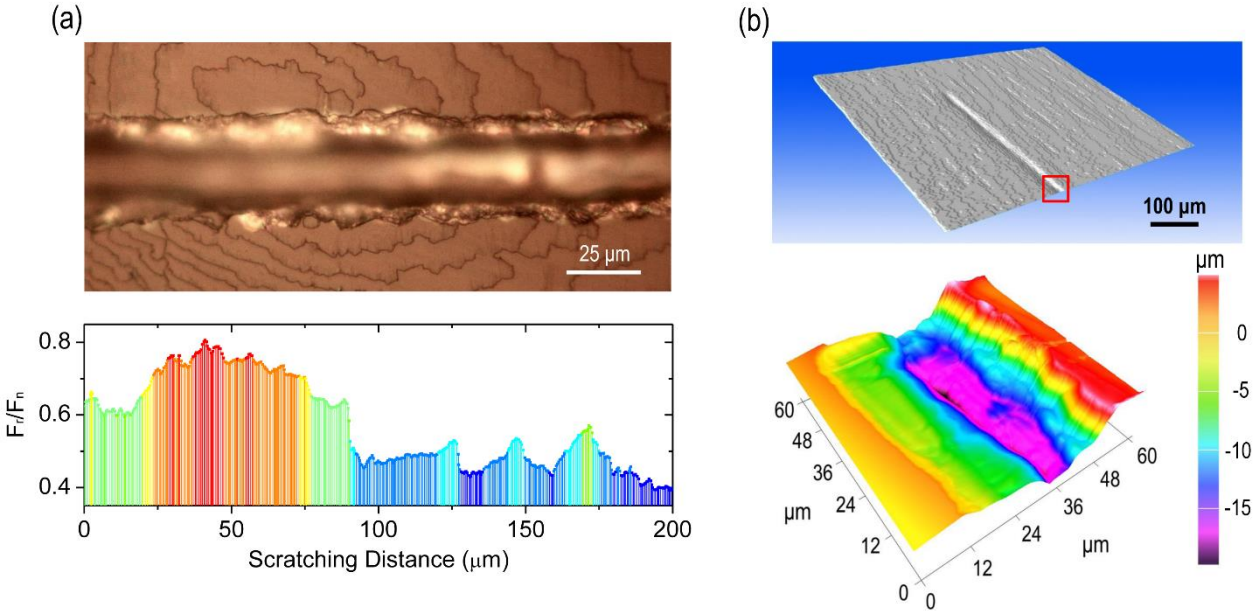

Fig. 3. (a) A scratch groove passing through a μ-SD and the corresponding real-time resistance force experienced by the probe. (b) The three-dimensional reconstruction of μ-CT model of the scratched surface and the depth contour of the scratch groove obtained by surface scanning (Hysitron Ti 900).

3. Numerical verification of the reinforcement of spiral interface

A virtual model of μ-SD is constructed by embedding a spiral interface (in green) into a cylinder (in gray), as shown in Fig. 4(a). In the accompanying Cartesian coordinate system (x, y, z), the spiral interface is described by parametric equations with respect to the polar coordinates (r, β) as

$$\begin{cases} x = r\cos\beta \\ y = r\sin\beta \\ z = p\beta/2\pi \end{cases} \quad \left(r \in [0, D/2] \text{ and } \beta \in [0, 2\pi l/p]\right), \tag{1}$$

where p is the spiral pitch, D and l denote the diameter and length of the specimen as indicated in Fig. 4(a). For comparison, a model of conventional laminated composite is also constructed by embedding

parallel planar interfaces separated by distance p into a similar cylinder, as shown in Fig. 4(b). Take D=18 μm, l =15 μm and p=1 μm. It can be demonstrated that the relative difference between the interface area in both models is less than 0.2 %, implying much alike compositions in both composites. Displacement-controlled uniaxial tension was simulated with commercial FEA package ABAQUS (Version 6.13, Dassault Systèmes). In our simulations, the laminae were depicted as linear elastic solid with elastic modulus E_{la} = 100 GPa (Song et al., 2003; Tushtev et al., 2008) and Poisson's ratio being 0.33. As the organic layer in the biological laminated composites is normally much thinner than the mineral lamina, cohesive element (COH3D8 in ABAQUS) with zero initial thickness was applied to describe the interface between laminae. By referring to the reported properties of the organic material in the biological laminated composites (Dastjerdi et al., 2013), we take the characteristic parameters of the cohesive element in our simulation as typical values shown in Table 1.

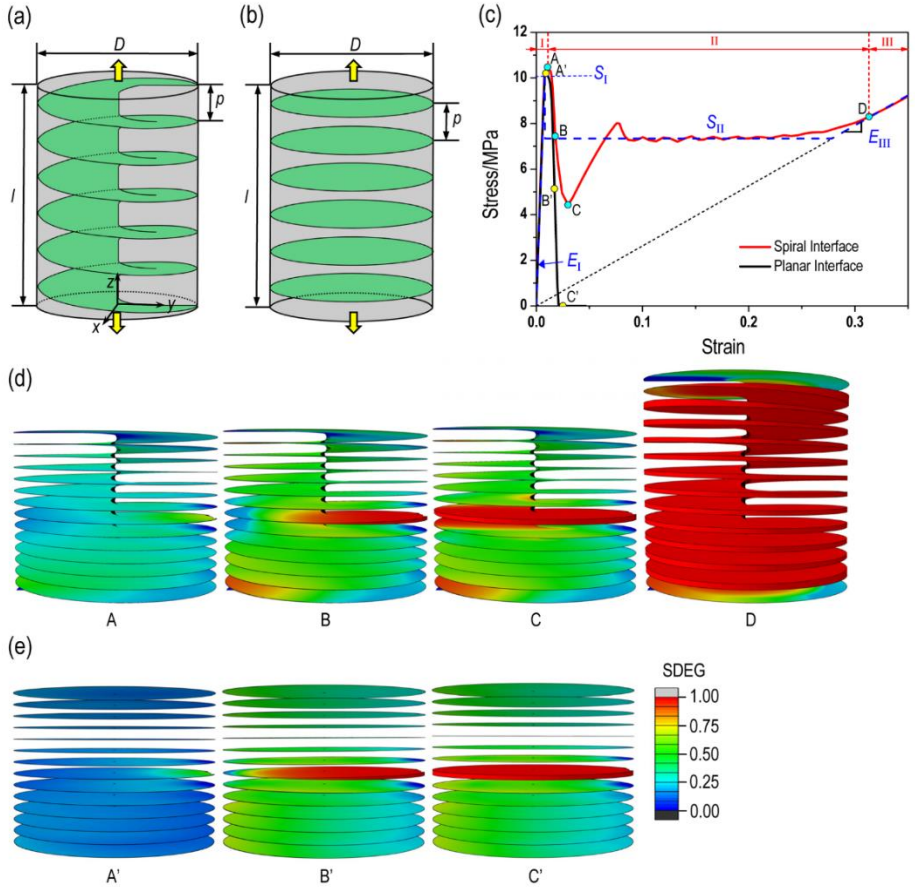

Fig. 4. Schematics of finite element models for laminated composites with (a) spiral and (b) parallel planar interfaces. D=18 μm, l =15 μm and p=1 μm; (c) Calculated stress-strain curves for two models under uniaxial tension. S_I, S_{II}, E_I and E_{III} are the characteristic mechanical properties of μ-SD

predicted by theory; (d, e) Snapshots of the SDEG (scalar stiffness degradation variable) field at different moments as indicated on the stress-strain curves in (c) showing the evolution of the interface damage. The deep blue color (SDEG=0) represents zero damage while the deep red color (SDEG=1.0) stands for the complete damage. For clarity, the lamina phase is hidden here.

Table 1. Characteristic parameters of cohesive elements (COH3D8 in ABAQUS) adopted in the finite element simulations

Stiffness K_{in} (GPa/μm)	Fracture energy G_{in} (J/m^2)	Strength S_{in} (MPa)
1.25	1.0	10

Fig. 4(c-e) shows the calculated stress-strain curves in company with the snapshots of the interface degradation at several important moments. For the composite with spiral interface (μ-SD), the stress-strain curve exhibits three characteristic stages (see Fig. 4(c)). At stage I when the deformation is relatively small, the stress increases linearly with the strain. Theoretical prediction (see Appendix A.1) indicates that the effective elastic modulus in stage I is given by

$$E_{\mathrm{I}} = \left(\frac{1}{E_{\mathrm{la}}} + \frac{1}{2E_{\mathrm{la}} p^2 \Big/ (\mathrm{Q}\pi D\sqrt{\pi^2 D^2 + p^2}) + K_{\mathrm{in}} p} \right)^{-1}, \tag{2}$$

where Q is a correction factor determined to be around 2.4 from our simulation. Such linear elasticity ends when the strain reaches a value around 1% at point A, giving rise to the strength of ~10.5 MPa. This value is quite close to its theoretical prediction (see Appendix A.2)

$$S_{\mathrm{I}} = S_{\mathrm{in}} \left(1 + \frac{2pE_{\mathrm{la}}}{Q\pi D K_{\mathrm{in}} \sqrt{\pi^2 D^2 + p^2}} \right), \tag{3}$$

which gives S_{I} =10.2 MPa according to the associated parameters we selected. After reaching the summit A, the stress drops quickly to ~4.4 MPa. An in-depth investigation into the status of cohesive elements indicates that such a drop of load-carrying capacity is basically due to the yielding and subsequent delamination of the interface, as shown in Fig. 4(d). With the growth of the delaminated spiral interface, the stress is maintained almost at a steady level even though small oscillation is present. This steady stress level can be deemed as the strength at stage II, which can be estimated analytically

as (see Appendix A.3)

$$S_{\mathrm{II}} = \sqrt{\frac{2G_{\mathrm{in}}}{\dfrac{Q\pi DK_{\mathrm{in}}\sqrt{\pi^2D^2+p^2}\,/(2pE_{\mathrm{la}})}{2pE_{\mathrm{la}}\,/(Q\pi D\sqrt{\pi^2D^2+p^2})+K_{\mathrm{in}}}-\dfrac{p}{E_{\mathrm{la}}}}}\,. \tag{4}$$

By substituting the values of the associated parameters into Eq. (4), we have S_{II} = 7.3 MPa which is in good agreement with the simulation result, as shown in Fig. 4(c). The ratio of $S_{\mathrm{II}}/S_{\mathrm{I}}$, which can be deemed as a yardstick for measuring the reinforcing effect of μ-SD, is shown in Fig. 5. For a given ratio D/p, $S_{\mathrm{II}}/S_{\mathrm{I}}$ decreases with increasing D, implying strong size dependence of the reinforcement. The smaller the μ-SD, the higher the reinforcement.

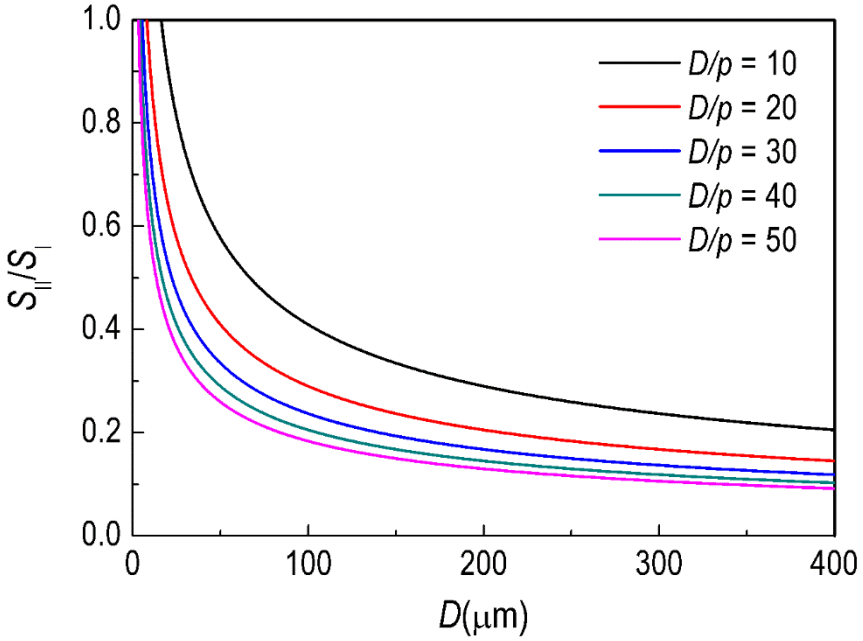

Fig. 5. Dependence of $S_{\mathrm{II}}/S_{\mathrm{I}}$ of a μ-SD on the length scale characterized by D. Here, following representative values are taken: G_{in} =1.0 J/m^2, K_{in}=1.25 GPa/ μm, S_{in}=10 MPa, E_{la}=100 GPa and Q =2.4.

With the increase of deformation, eventually the spiral interface is completely damaged at point D. From then on, deformation enters into stage III, in which linear elasticity returns with the effective elastic modulus predicted as (see Appendix A.4):

$$E_{\mathrm{III}} = \frac{2p^2}{Q\pi D\sqrt{\pi^2D^2+p^2}}E_{\mathrm{la}}\,. \tag{5}$$

By inserting the values of the associated parameters into Eq. (5), E_{III} is estimated to be around 26.1 MPa, which is in good consistency with the simulation result, as shown in Fig. 4(c). Such linear elasticity at stage III lasts all along until the damage of the lamina material, which has not been considered in our analysis.

In contrast, for the composite with planar interfaces, the calculated stress-strain curve in Fig. 4(c) exhibits a much more brittle behavior. Firstly, when the strain is smaller than 1%, a linear elasticity is also observed with elastic modulus given by (see Appendix B):

$$E_{\text{planar}} = \left(\frac{1}{E_{\text{la}}} + \frac{1}{K_{\text{in}} p} \right)^{-1}, \tag{6}$$

which is quite close to E_{I} in Eq. (2) when $D >> p$. After reaching the peak at point A', the stress drops abruptly to zero (point C'). Such catastrophic failure of the material is basically due to the propagation of the crack throughout a planar interface, as shown in Fig. 4(e). The distinct mechanical behaviors of laminated composites with spiral and planar interfaces in Fig. 4(c) confirm the reinforcing effect of μ-SD.

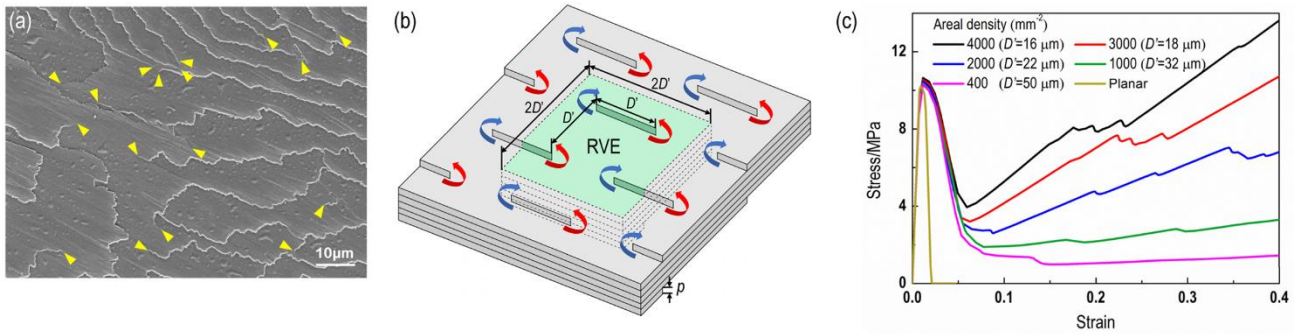

Fig. 6. (a) SEM image of an area (90 μm × 70 μm) on shell of *P. Placenta* containing 17 μ-SDs as marked by the yellow arrows. The areal density is estimated to be ≈ 2,700 mm^{-2}. (b) Schematics of an idealized composite model containing periodically distributed μ-SD couples. A representative volume element (RVE) with dimensions of $2D' \times 2D'$ is highlighted in green. (c) Calculated stress-strain curves for composites with μ-SDs of different areal densities using the RVE model shown in (b).

Above analysis demonstrated the reinforcement of an individual μ-SD. To shed light on the effect of multiple μ-SDs on the mechanical behavior of laminated composites, the density of μ-SDs should

be considered. An earlier study (Li and Ortiz, 2015) indicated that the areal density of μ-SDs in the shell of *P. Placenta* is about 100-400 mm^{-2}. However, our reexamination indicated that this might be the average density of μ-SDs over a relatively large area. For a smaller region, the local density of μ-SDs could reach 1,000-4,000 mm^{-2}, which is one order of magnitude higher than the above mean value. Fig. 6(a) shows a region containing 17 μ-SDs. The local density is estimated to be 2,700 mm^{-2}. For simplicity, our study on the effect of density was carried out by using an idealized model in which the distribution of μ-SDs was assumed periodical (see Fig. 6(b)). A RVE model with dimensions of $2D' \times 2D'$ was selected for analysis with periodical boundary conditions applied on four lateral sides. By applying uniaxial tension on the top and bottom sides, the mechanical behavior of a composite with μ-SD density of $1/D'^2$ is simulated. The calculated stress-strain curves for composites with different areal densities of μ-SD are shown in Fig. 6(c). As in the case of individual μ-SD (Fig. 4(c)), three characteristic stages are observed in the cases with high densities (e.g., 2,000, 3,000, 4,000 mm^{-2}), implying the operation of the reinforcing mechanism of μ-SDs. In contrast, for the case with density as low as 400 mm^{-2}, the stress drops abruptly from the maximum to a quite low value. Recovery of stress to a higher level does not happen as in the cases with high densities, implying little reinforcement as in the case with planar interfaces. Therefore, the reinforcement of the spiral interface in the laminated composites depends on the μ-SD density very much. The higher the density the higher the reinforcement. Certainly, this conclusion cannot be extended unlimitedly as the density of μ-SD should not be unpractically large; otherwise the assumption of laminated composite should not be valid any more. A reasonable estimation to the upper limit of the μ-SD density can be made based on the condition for laminated composite, say, $D'/p \geq 10$. In that case, the upper limit of the density is around $1/D'^2$ or $1/100p^2$, which equals 10,000 mm^{-2} if p is taken as 1μm.

4. Working condition for the reinforcing mechanism of μ-SD

The enhancement of μ-SDs to the mechanical properties of laminated composites shown above

is mainly attributed to the spiral interface which could guide the crack to propagate along a prolonged helical path. Clearly, this is not always the case because if the interface is much tougher compared to the lamina material, most likely a growing interfacial crack will deviate from the interface and penetrate into the laminae. Preventing the deviation of a growing interfacial crack from the spiral interface is crucial for ensuring the operation of the underlying reinforcing mechanism. For this purpose, a theoretical model was developed by analogizing the frontier of a spiral interfacial crack (see Fig. 7(a)) to a 2D (plane strain) crack under mixed mode loading (see Fig. 7(b)). The problem now comes down to finding the condition for ensuring the propagation of an interfacial crack along the interface under any external mixed-mode loading.

For a mixed-mode crack shown in Fig. 7(b), the directional dependence of the energy release rate at the crack tip is given by (Chang et al., 2006)

$$G(\theta)=\frac{1}{2\mu}\cos^2\frac{\theta}{2}\left\{\frac{\kappa+1}{8}\left[K_{\mathrm{I}}^2(1+\cos\theta)-4K_{\mathrm{I}}K_{\mathrm{II}}\sin\theta+K_{\mathrm{II}}^2(5-3\cos\theta)\right]+K_{\mathrm{III}}^2\right\}, \tag{7}$$

where θ denotes the direction angle with respect to the preexisting crack plane, μ is the shear modulus, and $\kappa=3-4\nu$ for plane strain with ν being the Poisson's ratio of the material. K_i represents the stress intensity factor of mode i (i = I, II, III).

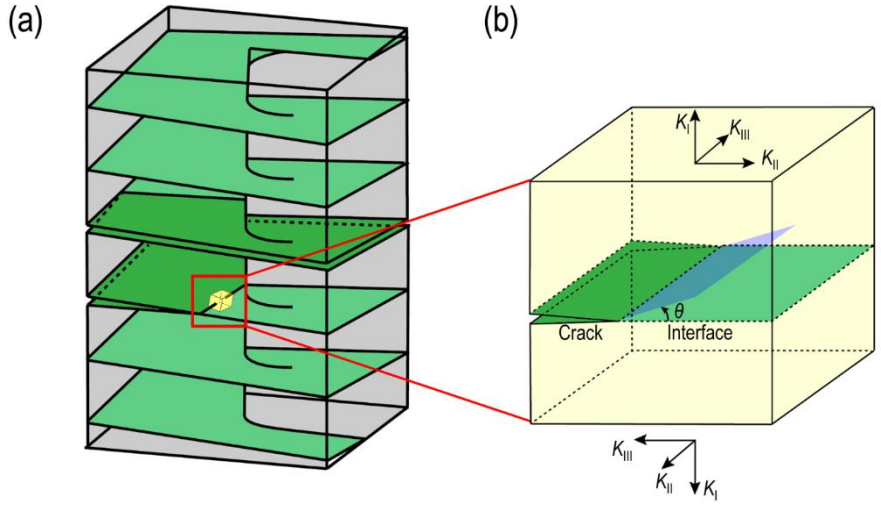

Fig. 7. The crack frontier of a spiral interface in (a) is equated to a 2D (plane strain) mixed-mode crack shown in (b).

Introduce two *mode ratio angles* defined by $\alpha = \tan^{-1}\left(K_{\mathrm{II}}/K_{\mathrm{I}}\right)$ and $\phi = \tan^{-1}\left(K_{\mathrm{III}}\Big/\sqrt{K_{\mathrm{I}}^2 + K_{\mathrm{II}}^2}\right)$ to correlate the loadings of different modes. Then the stress intensity factors can be expressed in terms of α and ϕ as

$$\begin{aligned} K_{\mathrm{I}} &= K_{\mathrm{all}}\cos\alpha\cdot\cos\phi, \\ K_{\mathrm{II}} &= K_{\mathrm{all}}\sin\alpha\cdot\cos\phi, \\ K_{\mathrm{III}} &= K_{\mathrm{all}}\sin\phi \end{aligned} \tag{8}$$

where $K_{\mathrm{all}} = \sqrt{K_{\mathrm{I}}^2 + K_{\mathrm{II}}^2 + K_{\mathrm{III}}^2}$. Thus, Eq. (7) can be rewritten in terms of K_{all}, α and ϕ as

$$G(\theta) = \frac{K_{\mathrm{all}}^2\cos^2(\theta/2)}{2\mu}\left\{\frac{\kappa+1}{8}\left[(1+\cos\theta)\cos^2\alpha - 2\sin 2\alpha\sin\theta + \sin^2\alpha(5-3\cos\theta)\right]\cos^2\phi + \sin^2\phi\right\}. \tag{9}$$

Assume crack propagates along the interface ($\theta = 0$). According to the Griffith criterion (Griffith, 1921), crack propagation happens when K_{all} reaches the critical value $K_{\mathrm{all\text{-}in}}$ satisfying the following condition:

$$G(\alpha,\phi,\theta=0,K_{\mathrm{all\text{-}in}}) = \frac{K_{\mathrm{all\text{-}in}}^2}{2\mu}\left(\frac{\kappa+1}{4}\cos^2\phi + \sin^2\phi\right) = G_{\mathrm{in}}, \tag{10}$$

where G_{in} represents the fracture toughness of the interface.

If the crack deflects and penetrates into the lamina material, according to the maximum energy release rate criterion (Chang et al., 2006), the fracture angle θ^* is determined by following conditions:

$$\left.\frac{\partial G(\theta)}{\partial\theta}\right|_{\theta=\theta^*} = 0 \quad \left(\text{with } \left.\frac{\partial^2 G(\theta)}{\partial\theta^2}\right|_{\theta=\theta^*} < 0\right). \tag{11}$$

In accordance with the Griffith criterion, crack propagation along θ^* direction happens when the load K_{all} reaches the critical value $K_{\mathrm{all\text{-}la}}$ satisfying following condition

$$\begin{aligned} &G(\alpha,\phi,\theta^*(\alpha,\phi),K_{\mathrm{all\text{-}la}}) \\ &= \frac{K_{\mathrm{all\text{-}la}}^2\cos^2(\theta^*/2)}{2\mu}\left\{\frac{\kappa+1}{8}\left[(1+\cos\theta^*)\cos^2\alpha - 2\sin 2\alpha\sin\theta^* + \sin^2\alpha(5-3\cos\theta^*)\right]\cos^2\phi + \sin^2\phi\right\} = G_{\mathrm{la}}, \end{aligned} \tag{12}$$

where G_{la} represents the fracture toughness of the lamina material. Preference of crack propagation along the interface requires

$$K_{\text{all-in}}^2 / K_{\text{all-la}}^2 < 1. \tag{13}$$

Substituting Eqs. (10) and (12) into (13) gives rise to

$$\frac{K_{\text{all-in}}^2}{K_{\text{all-la}}^2} = \frac{G_{\text{in}}}{G_{\text{la}}} \cdot \frac{G\left(\alpha, \phi, \theta^*(\alpha,\phi)\right)}{G\left(\alpha, \phi, \theta = 0\right)} < 1. \tag{14}$$

To satisfy the above condition for arbitrary α and ϕ, the maximum value of function

$$f\left(\alpha, \phi, \theta^*(\alpha,\phi)\right) = \frac{G\left(\alpha, \phi, \theta^*(\alpha,\phi)\right)}{G\left(\alpha, \phi, \theta = 0\right)} \tag{15}$$

is expected, which can be determined by solving equations

$$\begin{aligned} \frac{\partial f}{\partial \alpha} &= f'_{\alpha}\left(\alpha, \phi, \theta^*(\alpha,\phi)\right) + f'_{\theta^*}\left(\alpha, \phi, \theta^*(\alpha,\phi)\right) \cdot \frac{\partial \theta^*}{\partial \alpha} = 0, \\ \frac{\partial f}{\partial \phi} &= f'_{\phi}\left(\alpha, \phi, \theta^*(\alpha,\phi)\right) + f'_{\theta^*}\left(\alpha, \phi, \theta^*(\alpha,\phi)\right) \cdot \frac{\partial \theta^*}{\partial \phi} = 0. \end{aligned} \tag{16}$$

Since Eq. (11) implies that

$$f'_{\theta^*}\left(\alpha, \phi, \theta^*(\alpha,\phi)\right) = \frac{G'_{\theta^*}\left(\alpha, \phi, \theta^*(\alpha,\phi), K_{\text{all}}\right)}{G\left(\alpha, \phi, \theta = 0, K_{\text{all}}\right)} = 0, \tag{17}$$

Eq. (16) can be further simplified to be

$$\begin{aligned} \frac{\partial f}{\partial \alpha} &= f'_{\alpha}\left(\alpha, \phi, \theta^*(\alpha,\phi)\right) = 0, \\ \frac{\partial f}{\partial \phi} &= f'_{\phi}\left(\alpha, \phi, \theta^*(\alpha,\phi)\right) = 0. \end{aligned} \tag{18}$$

Solving Eqs. (11) and (18) for α, ϕ and θ^*, we have $\alpha = 60°$, $\phi = 0°$ and $\theta^* = -60°$. The maximum value of function f thus is given by

$$f_{\max} = f\left(\alpha = 60^\circ, \phi = 0^\circ, \theta^* = -60^\circ\right) \approx 1.69. \tag{19}$$

Therefore, Eq. (14) always holds as long as

$$\frac{G_{\text{in}}}{G_{\text{la}}} < \frac{1}{f_{\max}} \approx 0.6. \tag{20}$$

That is, if the fracture toughness of interface is less than 60% of that of the lamina, crack initiated on the interface will always grow along the interface irrespective of the direction of external loading. The operation of the enhancing mechanism of spiral interface and μ-SD thus is ensured.

5. Conclusion

In this paper, the mechanical behavior of μ-SD, a type of helical structure in biological laminated composites, was systematically studied. Analysis on an individual μ-SD showed that the failure of the μ-SD under tension involves the delamination of the prolonged spiral interface, giving rise to much higher toughness compared to those of the planar counterpart. Moreover, the corporation of multiple μ-SDs was investigated by studying the effect of μ-SD density on the mechanical reinforcement. It was found that the reinforcing effect was highly dependent on the density of μ-SDs. The higher the density, the higher the reinforcement. The operation of such reinforcing mechanism of μ-SD requires the delamination of spiral interface, which is not spontaneous but conditional. Theoretical modeling revealed that the proclivity of crack propagation along the spiral interface can be ensured if the fracture toughness of the interface is less than 60% of that of the lamina material. These findings not only uncover the reinforcing mechanisms of the μ-SDs in biological materials but also imply promising application of μ-SDs in reinforcing the synthetic laminated composites in engineering.

Acknowledgments

Supports for this work from the General Research Fund (GRF) of Hong Kong RGC (PolyU 152193/14E) and Central Research Grant from The Hong Kong Polytechnic University (PolyU 152481/16E) are acknowledged.

Appendix A: Prediction of mechanical behavior of μ-SD under uniaxial tension

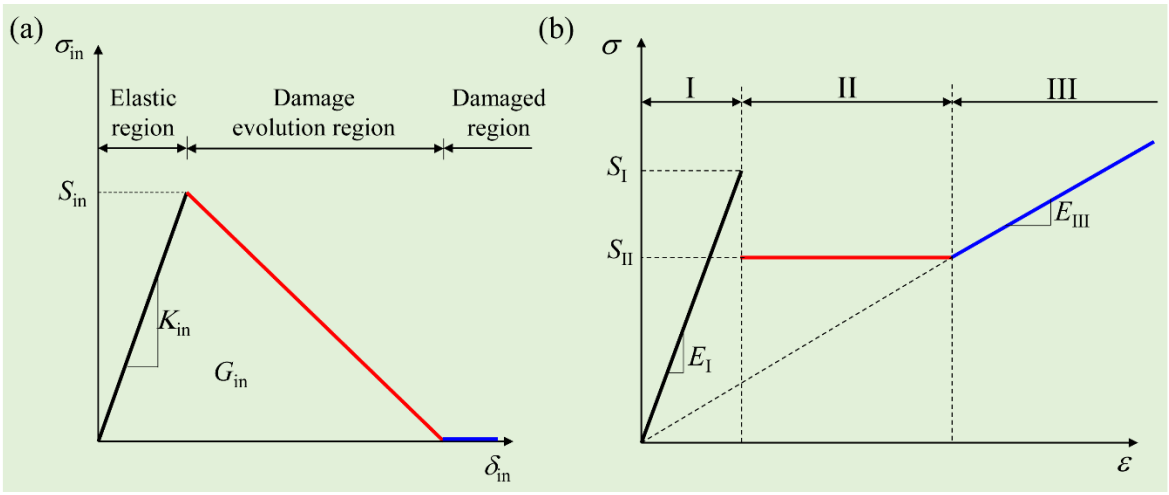

Fig. A1. (a) Schematics of traction-separation law for bilinear cohesive elements modelling adhesive interface, (b) Schematic stress-strain curve of μ-SD under uniaxial tension.

A μ-SD is a composite of a spiral lamina and interfacial adhesive. We assume lamina is elastic solid and interface can be described by a traction-separation law shown in Fig. A1(a). A μ-SD under uniaxial tension is believed to experience three distinct stages of deformation as depicted by three characteristic segments on a schematic stress-strain plot (see Fig. A1(b)). At stage I, both the spiral lamina and interface deform elastically, leading to the elastic behavior of the composite characterized by the effective elastic modulus E_I. With the increase of deformation, such elasticity continues until the interfacial traction reaches its maximum allowable value S_{in} (see Fig. A1(a)), giving rise to the strength S_I of the μ-SD at stage I (see Fig. A1(b)). From then on, interfacial delamination starts, resulting in a drop of load-bearing capacity of the μ-SD. However, due to the spiral morphology of the interface, interfacial delamination will not propagate thoroughly across the μ-SD as that in the regular laminated composite. Instead, it will grow progressively along a spiral path under stress S_{II} which gives rise to the strength of the μ-SD at stage II. Once the spiral interface delaminates completely, the μ-SD turns to be a monolithic spiral structure. Afterward, the μ-SD is expected to deform elastically with effective elastic modulus being E_{III}. In the following, theoretical estimations of E_I, S_I, S_{II} and E_{III} are carried out.

A.1 Theoretical prediction of the elastic modulus of μ-SD in stage I (E_I)

The effective elastic modulus of a μ-SD with intact interface (E_{I}) should be a function of the effective elastic modulus of interface ($K_{\mathrm{in}}p$, see Appendix B for derivation), the effective modulus of the plain spiral structure (E_{III}, see Section A.4 for derivation), and the elastic modulus of lamina materials (E_{la}). To shed light on the form of this function, discussion on its asymptotic values is helpful. Clearly, if the interface stiffness is quite large ($K_{\mathrm{in}} \to \infty$), no separation is allowed before the initiation of damage. Therefore, the μ-SD behaves like a monolithic cylinder made of the lamina material, implying that E_{I} approaches E_{la} as $K_{\mathrm{in}} \to \infty$. On the other hand, if $K_{\mathrm{in}} \to 0$, E_{I} must approach to the effective elastic modulus of μ-SD with completely failed interface (E_{III}). These two asymptotic properties of E_{I} in combination with the basic mixture laws of composites (Reuss, 1929; Voigt, 1889) inspire us to write E_{I} in the following form

$$E_{\mathrm{I}} = \left(\frac{1}{E_{\mathrm{la}}} + \frac{1}{E_{\mathrm{III}} + K_{\mathrm{in}} p} \right)^{-1}. \tag{A1}$$

It can be verified from Eq. (A1) that $E_{\mathrm{I}} \to E_{\mathrm{la}}$ as $K_{\mathrm{in}} \to \infty$, and $E_{\mathrm{I}} \to \left(\frac{1}{E_{\mathrm{la}}} + \frac{1}{E_{\mathrm{III}}} \right)^{-1}$ as $K_{\mathrm{in}} \to 0$.

Considering $p/D \ll 1$, the expression of E_{III} (see Section A.4) implies that $E_{\mathrm{III}} \ll E_{\mathrm{la}}$. Therefore, $E_{\mathrm{I}} \to E_{\mathrm{III}}$ as $K_{\mathrm{in}} \to 0$. Two asymptotic values of E_{I} are both confirmed. Inserting the expression of E_{III} (see Section A.4) into Eq. (A1), E_{I} can be rewritten as

$$E_{\mathrm{I}} = \left(\frac{1}{E_{\mathrm{la}}} + \frac{1}{2E_{\mathrm{la}} p^2 \Big/ (\mathrm{Q}\pi D\sqrt{\pi^2 D^2 + p^2}) + K_{\mathrm{in}} p} \right)^{-1}. \tag{A2}$$

A.2 Theoretical prediction of the strength of μ-SD in stage I (S_{I})

The maximum stress that a μ-SD can sustain before the initiation of damage of the included spiral interface contains two portions. One is the portion to overcome the maximum interfacial traction, which is equal to the strength of interface (S_{in}). The other portion is to deform the spiral solid to such an extent that makes the interfacial traction reach its maximum S_{in}. Since the interfacial separation at the maximum traction is $S_{\mathrm{in}}/K_{\mathrm{in}}$ (see Fig. A1(a)), the effective strain of the spiral solid with effective

modulus E_{III} is $S_{\mathrm{in}}/K_{\mathrm{in}}p$, implying that the stress required for such deformation is $S_{\mathrm{in}}E_{\mathrm{III}}/K_{\mathrm{in}}p$. Therefore, we have

$$S_{\mathrm{I}} = S_{\mathrm{in}} + \frac{S_{\mathrm{in}}E_{\mathrm{III}}}{K_{\mathrm{in}}p} = S_{\mathrm{in}}\left(1+\frac{E_{\mathrm{III}}}{K_{\mathrm{in}}p}\right). \tag{A3}$$

Since $E_{\mathrm{III}} = \dfrac{2p^2}{Q\pi D\sqrt{\pi^2D^2+p^2}}E_{\mathrm{la}}$ (see Section A.4), S_{I} can be rewritten as

$$S_{\mathrm{I}} = S_{\mathrm{in}}\left(1+\frac{2pE_{\mathrm{la}}}{Q\pi DK_{\mathrm{in}}\sqrt{\pi^2D^2+p^2}}\right). \tag{A4}$$

A.3 Theoretical prediction of the strength of μ-SD in stage II (S_{II})

In stage II, the spiral interface of μ-SD delaminates progressively under the tensile loading of S_{II}. From the point of view of energy equilibrium, during this process the energy required to fracture the interface should be equal to the released strain energy of a unit segment of μ-SD transforming from intact state to delaminated state. We therefore have

$$G_{\mathrm{in}} = \left(\frac{S_{\mathrm{II}}^2}{2E_{\mathrm{III}}} - \frac{S_{\mathrm{II}}^2}{2E_{\mathrm{I}}}\right)p, \tag{A5}$$

where G_{in} is the fracture energy of interface. From Eq. (A5), the strength of μ-SD in stage II (S_{II}) is thus given by

$$S_{\mathrm{II}} = \sqrt{\frac{2G_{\mathrm{in}}E_{\mathrm{I}}E_{\mathrm{III}}}{p(E_{\mathrm{I}}-E_{\mathrm{III}})}}. \tag{A6}$$

By substituting Eq. (A2) and E_{III} (see Section A.4) into (A6), S_{II} can be given as

$$S_{\mathrm{II}} = \sqrt{\frac{2G_{\mathrm{in}}}{\dfrac{Q\pi DK_{\mathrm{in}}\sqrt{\pi^2D^2+p^2}}{2pE_{\mathrm{la}}}/(2pE_{\mathrm{la}}) + K_{\mathrm{in}}} - \frac{p}{E_{\mathrm{la}}}}}. \tag{A7}$$

A.4 Theoretical prediction of the elastic modulus of μ-SD at stage III (E_{III})

Once the spiral interface fails completely, the μ-SD turns to be a monolithic solid with spiral structure. To estimate its effective elastic modulus, E_{III}, a unit segment is considered as shown in Fig.

A2(a), from which we select an annular element with infinitesimal thickness d*r* for analysis. The free body diagram is shown in Fig. A2(b). Considering the analogy of this problem in mechanics to a clamped beam under transverse loading (see Fig. A2(b)), the correlation between the force, *dF*, and the resulting deflection δ can be easily established as

$$\delta = Q\frac{L^3 dF}{12E_{\mathrm{la}}I}, \tag{A8}$$

where Q is the correction factor to be determined by simulation, $I = p^3\mathrm{d}r/12$ and $L = \sqrt{p^2 + (2\pi r)^2}$ are the moment of inertia and length of the analogic beam with p being the pitch of the spiral structure. Eq. (A8) thus can be rewritten as

$$dF = \frac{\delta E_{\mathrm{la}} p^3}{Q\left[p^2 + (2\pi r)^2\right]^{3/2}}\mathrm{d}r. \tag{A9}$$

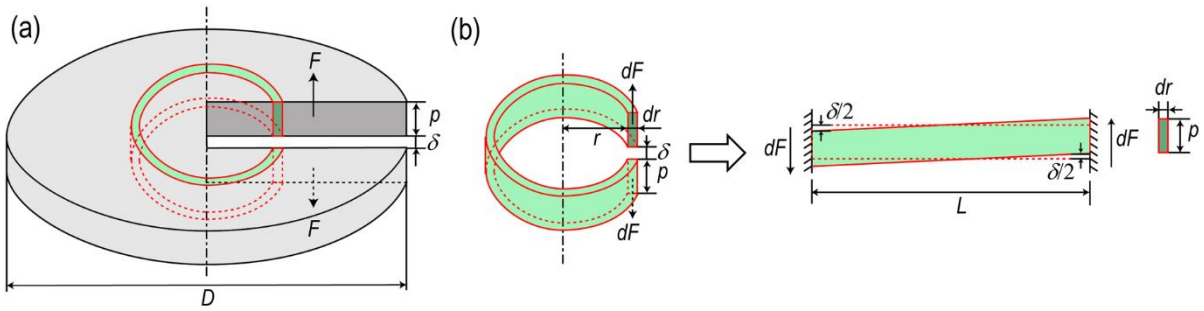

Fig. A2. (a) Schematics of a unit segment of μ-SD with failed interface. (b) Free body diagram of an annular element for analysis and its analogy.

Taking integration on both sides of Eq. (A9) gives rise to

$$F = \frac{E_{\mathrm{la}} p^3 \delta}{Q}\int_0^{D/2}\left[p^2 + (2\pi r)^2\right]^{-3/2}dr = \frac{E_{\mathrm{la}} Dp\delta}{2Q\sqrt{\pi^2 D^2 + p^2}}, \tag{A10}$$

where *D* is the diameter of the unit segment of μ-SD (see Fig. A2(a)). The effective modulus of μ-SD with completely failed interface can be determined as

$$E_{\mathrm{III}} = \frac{4F/(\pi D^2)}{\delta/p} = \frac{2p^2}{Q\pi D\sqrt{\pi^2 D^2 + p^2}}E_{\mathrm{la}}. \tag{A11}$$

When $D >> p$, Eq. (A11) can be further simplified as

$$E_{\mathrm{III}} \approx \frac{2p^2}{Q\pi^2 D^2} E_{\mathrm{la}}. \tag{A12}$$

Appendix B: Effective elastic modulus of regular laminated composite with planar interfaces (E_{planar})

Consider a laminated composite which is composed of planar laminae alternately bonded together by thin layers of adhesive substance (see Fig. 4(b)). We assume that the constitutive behavior of the adhesive interface between laminae can be described by a traction-separation law as shown in Fig. A1(a). Under external uniaxial loading σ, the axial elongation of a unit segment consisting of one lamina and one layer of adhesive interface is given by

$$\delta = \frac{\sigma}{E_{\mathrm{la}}} \cdot p + \delta_{\mathrm{in}}(\sigma), \tag{B1}$$

where E_{la} and p are the elastic modulus and thickness of the lamina, respectively; $\delta_{\mathrm{in}}(\sigma)$ is the interfacial separation of the adhesive under traction σ. The effective strain of the segment or the composite is given by

$$\varepsilon = \frac{\delta}{p} = \frac{\sigma}{E_{\mathrm{la}}} + \frac{\delta_{\mathrm{in}}(\sigma)}{p}. \tag{B2}$$

Here, the original thickness of the adhesive interface is neglected. The effective elastic modulus of the laminated composite with planar interfaces thus can be given by

$$E_{\mathrm{planar}} = \frac{\sigma}{\varepsilon} = \left(\frac{1}{E_{\mathrm{la}}} + \frac{\delta_{\mathrm{in}}(\sigma)}{p\sigma} \right)^{-1} = \left(\frac{1}{E_{\mathrm{la}}} + \frac{1}{K_{\mathrm{in}} p} \right)^{-1}, \tag{B3}$$

where K_{in} denotes the initial slope of the traction-separation curve for the interface (see Fig. A1(a)). In the light of Eq. (B3), it can be seen that $K_{\mathrm{in}} p$ represents the effective elastic modulus of the interface material.

References

Brunthaler, A., Reid, M.J., Menten, K.M., Zheng, X.W., Bartkiewicz, A., Choi, Y.K., Dame, T., Hachisuka, K., Immer, K., Moellenbrock, G., 2011. The bar and spiral structure Legacy (BeSSeL) survey: Mapping the Milky Way with VLBI astrometry. Astronomische Nachrichten 332, 461-466.

Chang, J., Xu, J.Q., Mutoh, Y., 2006. A general mixed-mode brittle fracture criterion for cracked materials. Engineering Fracture Mechanics 73, 1249-1263.

Dastjerdi, A.K., Rabiei, R., Barthelat, F., 2013. The weak interfaces within tough natural composites: experiments on three types of nacre. Journal of the Mechanical Behavior of Biomedical Materials 19, 50-60.

Gao, H., Ji, B., Jäger, I.L., Arzt, E., Fratzl, P., 2003. Materials become insensitive to flaws at nanoscale: lessons from nature. Proceedings of the National Academy of Sciences 100, 5597-5600.

Gibson, R.F., 1994. Principles of composite material mechanics. McGraw-Hill, United States.

Griffith, A.A., 1921. The phenomena of rupture and flow in solids. Philosophical Transactions of the Royal Society of London. Series A, Containing Papers of a Mathematical or Physical Character 221, 163-198.

Ji, B., Gao, H., 2004. Mechanical properties of nanostructure of biological materials. Journal of the Mechanics and Physics of Solids 52, 1963-1990.

Kelley, S.O., Barton, J.K., 1999. Electron transfer between bases in double helical DNA. Science 283, 375-381.

Li, L., Ortiz, C., 2015. A natural 3D interconnected laminated composite with enhanced damage resistance. Advanced Functional Materials 25, 3463-3471.

Mathai, A., Davis, T.A., 1974. Constructing the sunflower head. Mathematical Biosciences 20, 117-133.

Meyers, M.A., Lin, A.Y.-M., Chen, P.-Y., Muyco, J., 2008. Mechanical strength of abalone nacre: role of the soft organic layer. Journal of the Mechanical Behavior of Biomedical Materials 1, 76-85.

Reuss, A., 1929. Berechnung der fließgrenze von mischkristallen auf grund der plastizitätsbedingung für einkristalle. ZAMM - Journal of Applied Mathematics and Mechanics/Zeitschrift für Angewandte Mathematik und Mechanik 9, 49-58.

Shao, Y., Zhao, H., Feng, X., Gao, H., 2012. Discontinuous crack-bridging model for fracture toughness analysis of nacre. Journal of the Mechanics and Physics of Solids 60, 1400-1419.

Song, F., Soh, A., Bai, Y., 2003. Structural and mechanical properties of the organic matrix layers of nacre. Biomaterials 24, 3623-3631.

Tang, H., Barthelat, F., Espinosa, H., 2007. An elasto-viscoplastic interface model for investigating the constitutive behavior of nacre. Journal of the Mechanics and Physics of Solids 55, 1410-1438.

Taylor, G.I., 1934. The mechanism of plastic deformation of crystals. Part I. Theoretical. Proceedings of the Royal Society of London. Series A, Containing Papers of a Mathematical and Physical Character 145, 362-387.

Tushtev, K., Murck, M., Grathwohl, G., 2008. On the nature of the stiffness of nacre. Materials Science

and Engineering: C 28, 1164-1172.
Vogel, H., 1979. A better way to construct the sunflower head. Mathematical Biosciences 44, 179-189.
Voigt, W., 1889. Ueber die Beziehung zwischen den beiden Elasticitätsconstanten isotroper Körper. Annalen der physik 274, 573-587.
Wada, K., 1966. Spiral growth of nacre. Nature 211, 1427.
Wang, A., Quigley, G.J., Kolpak, F.J., Crawford, J.L., van Boom, J.H., van der Marel, G., Rich, A., 1979. Molecular structure of a left-handed double helical DNA fragment at atomic resolution. Nature 282, 680-686.
Wang, R.Z., Suo, Z., Evans, A.G., Yao, N., Aksay, I.A., 2001. Deformation mechanisms in nacre. Combustion Science & Technology 16, 2485-2493.
Watson, J.D., Crick, F.H., 1953. Molecular structure of nucleic acids. Nature 171, 737-738.
Weinberg, M.D., 1992. Detection of a large-scale stellar bar in the Milky Way. The Astrophysical Journal 384, 81-94.
Yao, N., Epstein, A., Akey, A., 2006. Crystal growth via spiral motion in abalone shell nacre. Journal of Materials Research 21, 1939-1946.
Yao, N., Epstein, A.K., Liu, W.W., Sauer, F., Yang, N., 2009. Organic-inorganic interfaces and spiral growth in nacre. Journal of the Royal Society Interface 6, 367-376.